

## Abstract



# Contents

<b>1</b>	<b>Introduction</b>	<b>5</b>
1.1	Quantum Computing . . . . .	5
1.2	Quantum Error Correction . . . . .	5
1.3	Weakly coupled carbons; a naturally occurring register . . . . .	5
<b>2</b>	<b>Electronic spins in Diamond</b>	<b>7</b>
2.1	Spin Control . . . . .	7
<b>3</b>	<b>Addressing Weakly-coupled Carbon Spins</b>	<b>9</b>
3.1	Hyperfine Coupling . . . . .	9
3.2	Addressing Weakly-coupled Carbons through Dynamical Decoupling . . . . .	10
3.3	Characterizing the Nuclear-spin environment . . . . .	11
<b>4</b>	<b>Controlling Weakly-coupled Carbon Spins</b>	<b>15</b>
4.1	Carbon control (more of a theory chapter, change title) . . . . .	15
4.2	Controlling weakly coupled carbons trough the electronic spin . . . . .	16
4.3	Carbon Initialization & Readout . . . . .	16
<b>5</b>	<b>Deterministic Parity Measurements</b>	<b>17</b>
5.1	Entanglement . . . . .	17
5.2	Verification of Entanglement . . . . .	17
<b>6</b>	<b>Outlook: towards Quantum Error Correction</b>	<b>19</b>
<b>A</b>	<b>Fingerprintdata</b>	<b>23</b>
<b>B</b>	<b>State Initialization</b>	<b>25</b>
<b>C</b>	<b>Bell State Tomography</b>	<b>27</b>
<b>D</b>	<b>Entanglement wittness</b>	<b>29</b>
<b>E</b>	<b>Simulations</b>	<b>31</b>



## 1.1 Quantum Computing

The idea of using a quantum mechanical system to simulate physics was first explored by Feynman[5]. Because the Hilbert space(/state space?) of a quantum mechanical system scales exponentially with it's size one would need an exponentially large classical computer to simulate it's behavior. By manipulating a quantum mechanical system directly this scaling problem can be circumvented.

It was quantum simulation that eventually led to the idea of exploiting quantum effects to perform more efficient calculations but it wasn't until Shor's discovery of a remarkably efficient quantum algorithm for prime factorization in 1994[12] that quantum information science really took off.

Shor's algorithm was the first example where a quantum computer can provide an exponential speedup over a classical computer. Shor's and other quantum algorithms allow solving classes of problems that were previously unsolvable, a well known example being the breaking of classical encryption codes.

By now Shor's algorithm has been shown to work on a range of different small scale quantum computers [17] [Needs reference to Shor in different systems or basic algorithms in range of systems] but making a scalable quantum computer that can take full advantage of the exponential speedup proves elusive.

## 1.2 Quantum Error Correction

## 1.3 Weakly coupled carbons; a naturally occurring register

The Nitrogen Vacancy centre in diamond is a well investigated system[4] and a promising candidate for quantum computation[2]. In order to implement three qubit measurement based QEC we need three qubits plus ancillae that we can initialise, measure and conditionally perform operations on. These extra qubits are found in Carbon-13 atoms, which are normally a source of decoherence. These atoms can be addressed using a resonant decoupling sequence[14].



## Electronic spins in Diamond

It has been shown that the nuclear- and electron- spin-state of the NV- center can be initialized, controlled and read-out using microwave- and laser- pulses[11]. In these experiments two lasers that are resonant with transitions in the NV- center are used to initialize the electronic spin state. One of these two lasers is used to read out the electronic spin state and an off-resonant laser is used to reset the system. Microwaves are used to drive transitions between the different nuclear and electronic spin states.

Strongly coupled nuclear spins can be initialized by conditionally rotating the electronic state to a state that is read out only if the Carbon is in the desired state, when the electronic state readout has a positive result the system is projected into the desired state. We call this Measurement Based Initialization (MBI). Our experiments are build around the same basic tools. Each experiment starts with a Charge-Resonance check that verifies if the lasers are still on resonance. After that the Nitrogen spin state is initialized using MBI. Once the system is initialized the actual experiment is performed. An experiment consists of one or multiple blocks of microwave pulses and optical readouts.

All experiments were performed on a custom-build cryostat setup operating at liquid helium temperatures described in detail in Bernien [1, chap. 3]. The setup was additionally outfitted with a movable neodymium magnet that applied a magnetic field of 300G to the sample.

### 2.1 Spin Control

The electronic ground state Hamiltonian can be written as[10]:

$$H_{GS} = \Delta S_z^2 + \gamma_e \mathbf{B} \cdot \mathbf{S} \quad (2.1)$$

With zero field splitting  $\Delta \approx 2.88\text{GHz}$  and gyro-magnetic ratio  $\gamma_e = 2.802 \text{ MHz/G}$ . In this expression the interactions with the nitrogen nucleus and the carbon spin bath are not included. By applying a magnetic field  $B_z$  along the NV-axis the degeneracy of the  $m_s = \pm 1$  states is lifted by the Zeeman effect. We define our electronic qubit by the two level system with  $m_s = 0 := |0\rangle$  and  $m_s = +1 := |1\rangle$ .

On the Bloch-sphere the state vector rotates around the quantization axis with a frequency depending on the energy splitting between the two states; the Larmor frequency. For the NV-electronic spin transition used the Larmor frequency is given by eq. (2.2).

$$\omega_L = \Delta + \gamma_e B_z \quad (2.2)$$

By applying an external field a term is effectively added to the Hamiltonian, changing the quantization axis and thereby its evolution. By applying microwaves with the right frequency this can be used to selectively drive the transition from the  $|0\rangle$  state to the  $|1\rangle$  state[9].





## Addressing Weakly-coupled Carbon Spins

Similar to how the electronic spin can be controlled by adding and removing a term to the Hamiltonian we can also control the state of a weakly-coupled carbon-13 atom. This chapter will start by providing theoretical background on the hyperfine coupling between carbon spins and the NV-center. The second section will explain how nuclear spins can be addressed. The next section will explain and show characterization of the nuclear spin environment. The last section will explain how carbon-spins can be controlled and will demonstrate initialization control and readout of weakly coupled carbon spins.

### 3.1 Hyperfine Coupling

The Hamiltonian of the nuclear spin depends on the electronic spin state and is given by eq. (3.1) when the electronic-spin is in the  $m_s = 0$  state and by eq. (3.2) when in the  $m_s = +1$  state for a magnetic field in the z-direction[16].

$$H_0 = \gamma_C B_z I_z \quad (3.1)$$

$$H_1 = \gamma_C B_z I_z + H_{\text{HF}} \quad (3.2)$$

The Larmor frequency for a carbon nucleus is given by eq. (3.3).

$$\omega_L = \gamma_C B \quad (3.3)$$

The hyperfine ( $H_{\text{HF}}$ ) term consists of a contact term and a dipole term. The contact term results from an overlap between the electronic- and carbon- wave-functions making it negligible for all but the carbon-spins closest to the NV-center. Hyperfine strengths between the NV-center and carbons on close-by lattice sites have been measured[13] and calculated[6, 7], as we are only interested in weakly coupled carbons the contact term of the hyperfine-interaction can be safely neglected.

We define a carbon to be weakly-coupled when its hyperfine coupling strength is much smaller than the Larmor frequency. For all practical magnetic fields this does not include the close-by carbons that have a contact term in their hyperfine-interaction. For weakly-coupled carbons the hyperfine-term is equal to the dipole-term and is given by eq. (3.4)[3].

$$H_{\text{dip}} = \frac{\mu_0 \gamma_e \gamma_C \hbar^2}{4\pi r^3} [\mathbf{S} \cdot \mathbf{I} - 3(\mathbf{S} \cdot \hat{n}_{\text{hf}})(\mathbf{I} \cdot \hat{n}_{\text{hf}})] \quad (3.4)$$

From eq. (3.4) the parallel and orthogonal components of the Hyperfine interaction, with respect to the NV-axis along the z-direction, can be derived to be:

$$A_{\parallel} = -\frac{\mu_0 \gamma_e \gamma_C \hbar^2}{4\pi r^3} \left( 3 \cdot \frac{z^2}{r^2} - 1 \right) \quad (3.5)$$

$$A_{\perp} = -\frac{\mu_0 \gamma_e \gamma_C \hbar^2}{4\pi r^3} \left( 3 \cdot \frac{\sqrt{x^2 + y^2} \cdot z}{r^2} \right) \quad (3.6)$$

Where  $H_{\text{dip}} = A_{\parallel} I_z + A_{\perp} I_x$ .

### 3.2 Addressing Weakly-coupled Carbons through Dynamical Decoupling

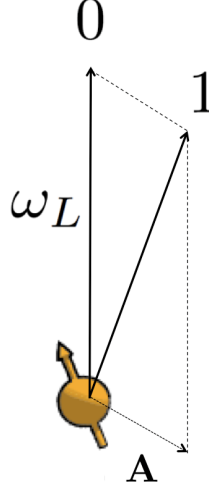


**Figure 3.1** – Flipping the electron spin from the  $m_s = 0$  to the  $m_s = +1$  state changes the quantization axis of  $^{13}\text{C}$  nuclear spins. For  $m_s = 0$  spins precess about  $\omega_L$ . For  $m_s = +1$  spins precess about a distinct axis  $\tilde{\omega} = \omega_L + \mathbf{A}$ .

Spins precess about a quantization axis along  $\tilde{\omega}$  with a frequency  $|\tilde{\omega}|$ . We call  $\tilde{\omega}$  the quantization-vector. When the electron is in the  $m_s = 0$  state each nuclear spin precesses about  $\tilde{\omega} = \omega_L$  with the Larmor frequency. The magnetic field is aligned along the quantization axis of the NV-center and defined as the z-direction. When the electron is in the  $m_s = +1$  state nuclear spins precess about a distinct axis  $\tilde{\omega} = \omega_L + \mathbf{A}$  [15]. The hyperfine interaction  $\mathbf{A}$  depends on the position of that particular nuclear spin relative to the NV- center.

To understand how a carbon-13 atom can be controlled it is useful to consider three situations. In the first situation the  $\omega_L$  and  $\mathbf{A}$  point in the same direction. In the second situation  $\omega_L$  and  $\mathbf{A}_\perp$  are of comparable magnitude, resulting in a large angle between the quantization axes. In the last situation  $|\mathbf{A}|$  is small compared to  $|\omega_L|$  resulting in a small angle between the quantization axes.

When applying a decoupling sequence with  $N/2$  decoupling units of the form  $\tau - \pi - 2\tau - \pi - \tau$ , with  $\tau$  a wait time between pulses, and  $\pi$  a  $\pi$ -pulse that flips the electron-state, the nuclear spin alternately rotates around the  $\omega_L$  and the  $\tilde{\omega}$  axis. The net result of one such decoupling sequence is a rotation around an axis  $\hat{\mathbf{n}}_i$  by an angle  $\phi$ . Where  $\hat{\mathbf{n}}_i$  depends on the initial state of the electron:  $\hat{\mathbf{n}}_0$  when the electron starts in  $m_s = 0$  and  $\hat{\mathbf{n}}_1$  when the electron starts in  $m_s = +1$  [15].

When  $\omega_L$  and  $\mathbf{A}$  point in the same direction, the net rotation axis is independent of the initial electron-state making it impossible to use the electron to control the carbon-13 atom using this decoupling sequence.

In the case where  $\omega_L$  and  $\mathbf{A}_\perp$  are of comparable magnitude the net rotation axes  $\hat{\mathbf{n}}_i$  are strongly dependent on the initial electron-state for almost any  $\tau$ . Having one of these carbon atoms can make it hard to selectively control other carbons as there are very few inter-pulse-delays  $2\tau$  for which only the carbon atom without the strong orthogonal-hyperfine is affected.

When considering the case where  $|\mathbf{A}|$  is small compared to  $|\omega_L|$  the net rotation axes  $\hat{\mathbf{n}}_0$  and  $\hat{\mathbf{n}}_1$  are practically parallel and the nuclear spin undergoes an unconditional evolution. Only when the inter-pulse delay is precisely resonant with the spin dynamics the axes are anti-parallel leading to a conditional rotation[15]. The resonant condition occurs at:

$$\tau = \frac{(2k+1)\pi}{2\gamma_C B_z + A_\parallel} \quad (3.7)$$

And for  $\omega_L \gg |\mathbf{A}|$  the dip has a width of:

$$\Delta = \frac{A_\perp}{2 \cdot (\gamma_C B_z)^2} \quad (3.8)$$

If  $\hat{\mathbf{n}}_0$  and  $\hat{\mathbf{n}}_1$  are not parallel, the resulting conditional rotation of the nuclear spin generally entangles the electron and nuclear spins. As a result, for an unpolarized nuclear spin state, the

final electron spin state is a statistical mixture of  $|x\rangle$  and  $|-x\rangle$  when starting from the  $|x\rangle$  state. Where the probability that the initial state is preserved is given by eq. (3.9). The contrast  $M_j$  for a single nuclear spin is given by eq. (3.10)[15].

$$P_x = (M + 1)/2 \quad (3.9)$$

$$M_j = 1 - (1 - \hat{\mathbf{n}}_0 \cdot \hat{\mathbf{n}}_1) \sin^2 \frac{N\phi}{2} \quad (3.10)$$

$$1 - \hat{\mathbf{n}}_0 \cdot \hat{\mathbf{n}}_1 = \frac{A_\perp^2}{\tilde{\omega}^2} \frac{(1 - \cos(\tilde{\omega}\tau))(1 - \cos(\omega_L\tau))}{1 + \cos(\tilde{\omega}\tau)\cos(\omega_L\tau) - (\frac{A_\parallel + \omega_L}{\tilde{\omega}})\sin(\tilde{\omega}\tau)\sin(\omega_L\tau)} \quad (3.11)$$

$$\phi = \cos^{-1} \left( \cos(\tilde{\omega}\tau)\cos(\omega_L\tau) - \left( \frac{A_\parallel + \omega_L}{\tilde{\omega}} \right) \sin(\tilde{\omega}\tau)\sin(\omega_L\tau) \right) \quad (3.12)$$

### 3.3 Characterizing the Nuclear-spin environment

#### Dynamical Decoupling Spectroscopy

In reality the electron is not interacting with a single carbon but with a bath of carbon atoms. When the electron interacts with multiple carbons at the same time the contrast  $M$  is given by the product of all individual values  $M_j$  for each individual spin  $j$  (eq. (3.13)). In order to selectively control one carbon the electron should not entangle with any other carbon when addressing it.

$$M = \prod_j M_j \quad (3.13)$$

To identify promising resonances for carbon control a dynamical decoupling spectroscopy experiment is performed, resulting in a fingerprint of the nuclear-spin environment[15]. In a dynamical decoupling spectroscopy experiment the electron is prepared in the  $|X\rangle = |0\rangle + |1\rangle$  state. It is subjected to a decoupling sequence consisting of  $N/2$  blocks of the form  $\tau - \pi - 2\tau - \pi - \tau$ , and concluded by measuring  $\langle X \rangle$ . The fingerprint is the result of many repetitions for a range of inter-pulse delays  $2\tau$ .

#### Contributions of Different Spins

A narrow dip in the fingerprint spectrum is an indication of a selectively addressable carbon. By sweeping the number of  $\pi$ -pulses on such a dip it can be verified if it corresponds to a *single* carbon. If entanglement is created with a lot of spins at once all coherence is lost and contrast will go to 0. Only if no entanglement is created with other carbons can the contrast be swepted to -1.

Because carbon-13 atoms are randomly distributed in diamond there is a wide range of possible hyperfine strengths. Most carbon-spins have very similar hyperfine-interaction strengths as they are relatively far away from the NV-center. This causes their resonances to overlap, manifesting itself as a broad feature with little coherence in the fingerprint. We identify this response as the spin-bath collapse.

Spins that have a stronger than average hyperfine-interaction show up outside or at the edge of the spin-bath collapse. Going to larger  $\tau$  separates resonances further as their order  $k$  increases, allowing for control of more spins. As computations are fundamentally limited by the coherence time there is a limit to the resonance-order that can be used to address carbons.

Some of the relatively strong-coupled spins have a strong orthogonal-component of the hyperfine interaction. This orthogonal-component causes a broad response, effectively blocking a large range of  $\tau$  from being used to control other spins.

#### Effect of the magnetic field

Both these issues can be alleviated by increasing the magnetic field. By increasing the magnetic field the Larmor frequency can be made much larger than the orthogonal components of the hyperfine interactions causing the broad resonances to disappear. Additionally increasing the magnetic field causes resonances to move closer to  $\tau = 0$  (eq. (3.7)), while at the same time

becoming narrower (eq. (3.8)), allowing higher order resonances to be addressed within the same time-window.

Increasing the magnetic field will not always improve the situation. When the magnetic field is too strong the resonances become narrower than the resolution of the Arbitrary Waveform Generator used to generate the pulses that address the resonances, making it impossible to address these resonances effectively. Simulations that were performed (see appendix E) indicate that for diamond with a natural concentration of carbon-13 there is a broad range between 400G and 1400G where the magnetic field is optimal.

There are also practical limitations to how much the magnetic field can be increased. In order to control carbon-spins we must still be able to coherently initialize, control and read-out the electronic-spin-state. Because the transitions used for read-out and initialization depend on strain and magnetic field[8], care must be taken when measuring at different magnetic fields that states do not mix in the excited state. This combined with the fact that few experiments have been performed at high magnetic field and low temperature make it more practical to settle for a more moderate magnetic field of 300G.

## Identifying Individual Carbon-spins

To identify spins a dynamical decoupling spectroscopy was performed on the sample with  $N = 8, 16, 32$  and  $64$  pulses. For  $N = 8, 16$  and  $32$  pulses this was done between  $\tau = 2\mu s$  and  $72\mu s$  and for  $N = 64$  this was done up to  $\tau = 52\mu s$ . We identify distinct features in the fingerprint and try to assign different hyperfine-couplings to them such that the computed data for these spins fits the measured data as well as possible. The response of a single spin is computed using eq. (3.10). 13 spins were identified using this method.

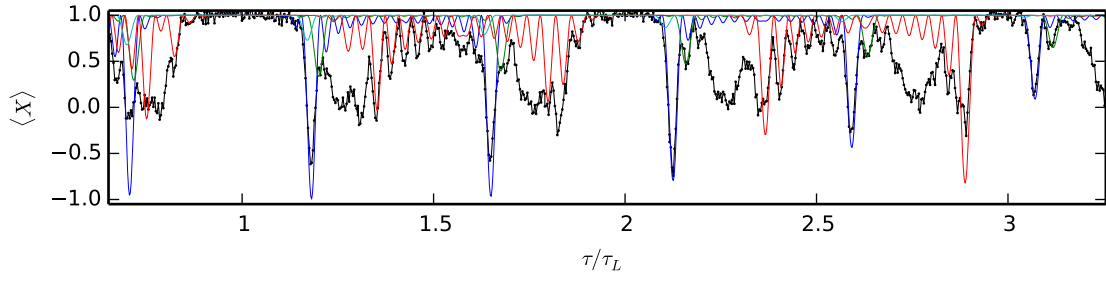
Figure 3.2 shows a subset of the fingerprint data acquired for this thesis. Table 3.1 shows the estimated hyperfine parameters of the 4 carbon spins with the strongest coupling. All estimated hyperfine parameters and a link to the full fingerprint measurements can be found in appendix A.

The broad collapse due to the spin bath is clearly visible at  $\tau/(4\tau_L)$  for odd  $m$ . The most prevalent feature of the spectrum is a strong oscillation between the spin-bath collapses. This oscillation can be explained by a single carbon that has a strong orthogonal hyperfine coupling, labeled spin-2 in our analysis. Due to the nature of spin-2 it is hard to find other carbons that can be coherently controlled.

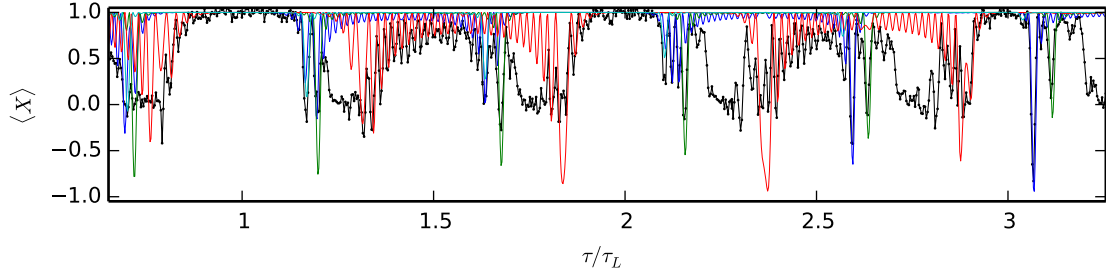
Nonetheless there are still some distinct peaks at the edge of the spin-bath collapse. When going to higher orders we see these peaks separate from the spin-bath response. We find that we can address 4 spins. These are listed in table 3.1.

Carbon	$A_{\parallel}$	$A_{\perp}$
1	$2\pi \cdot 30.0$ kHz	$2\pi \cdot 80.0$ kHz
2	$2\pi \cdot 27.0$ kHz	$2\pi \cdot 28.5$ kHz
3	$2\pi \cdot -51.0$ kHz	$2\pi \cdot 105.0$ kHz
4	$2\pi \cdot 45.1$ kHz	$2\pi \cdot 20.0$ kHz

**Table 3.1** – Estimated hyperfine parameters for spins 1 to 4 in fig. 3.2.



(a) Fingerprint for  $N=16$  pulses.



(b) Fingerprint for  $N=32$  pulses.

**Figure 3.2** – Part of a fingerprint resulting from a dynamical-decoupling-spectroscopy experiment performed at 304.12G. A reference to the full spectroscopy can be found in appendix A. Colored lines represent computed responses of carbon spins. Responses were calculated using eq. (3.10) with hyperfine parameters from table 3.1. NOTE: labels for colored spins still coming.



## Controlling Weakly-coupled Carbon Spins

### 4.1 Carbon control (more of a theory chapter, change title)

When on resonance (eq. (3.7)) the carbon rotates around one of two distinct anti-parallel axes based on the state the electron is in. [Need some statement that puts the axis in the equator when on resonance. Look in appendix again] We define the

Figure of Bloch sphere showing  $n_0$  and  $n_1$  axis. A state starting of in 0 being rotated to  $+y$  and  $-y$  ( $\pm x$  operation). Different arrow  
adf

Note the Bloch sphere is a model that cannot accurately represent the dynamics of a 2-qubit system. Nonetheless it can be a useful simplification in explaining qubit control. Test

More tests to see if it works

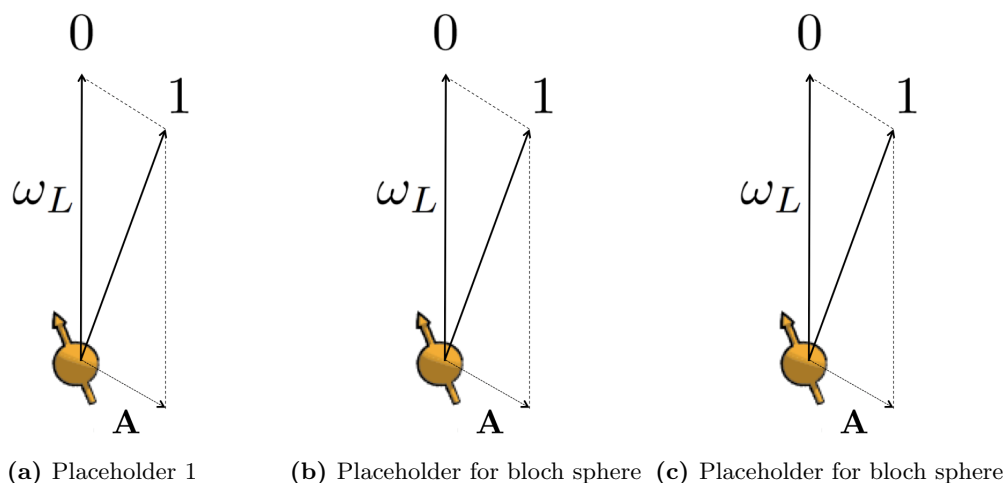


Figure 4.1 – Nuclear Ramsey experiment with

### Measuring Precession Frequencies

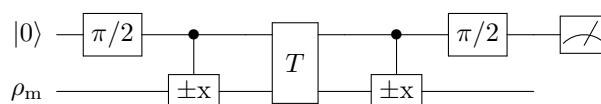
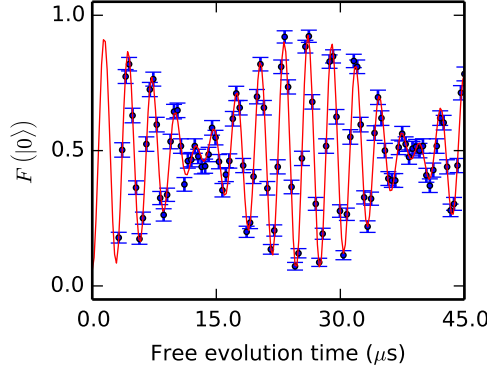
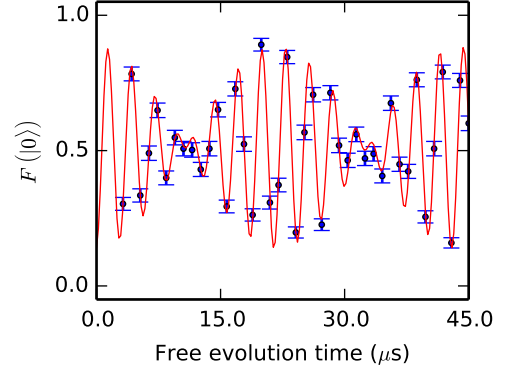


Figure 4.2 – Carbon Ramsey experiment.



(a) Nuclear Ramsey of Carbon 1



(b) Nuclear Ramsey of Carbon 4

Figure 4.3 – Nuclear Ramsey experiment wit

## 4.2 Controlling weakly coupled carbons trough the electronic spin

Explain how carbon control works in theory. Explain how a conditional and unconditional gate can be performed. Explain initialization on gate level, refer to appendix for calculations. Explain Readout.

## 4.3 Carbon Initialization & Readout

Show results that demonstrate carbon control.



## **Deterministic Parity Measurements**

### **5.1 Entanglement**

### **5.2 Verification of Entanglement**



## Outlook: towards Quantum Error Correction

Lorem ipsum dolor sit amet, consectetur adipisicing elit, sed do eiusmod tempor incididunt ut labore et dolore magna aliqua. Ut enim ad minim veniam, quis nostrud exercitation ullamco laboris nisi ut aliquip ex ea commodo consequat. Duis aute irure dolor in reprehenderit in voluptate velit esse cillum dolore eu fugiat nulla pariatur. Excepteur sint occaecat cupidatat non proident, sunt in culpa qui officia deserunt mollit anim id est laborum.



## Bibliography

- [1] H. Bernien. *Control, Measurement and Entanglement of Remote Quantum Spin Registers in Diamond*. PhD thesis, Delft University of Technology, 2014.
- [2] L. Childress and R. Hanson. Diamond nv centers for quantum computing and quantum networks. *MRS Bulletin*, 38(02):134–138, 2 2013. ISSN 0883-7694. URL [http://www.journals.cambridge.org/abstract\\_S0883769413000201](http://www.journals.cambridge.org/abstract_S0883769413000201).
- [3] G. de Lange. *Quantum Control and Coherence of Interacting Spins in Diamond*. PhD thesis, Delft University of Technology, 2012.
- [4] M.W. Doherty, N.B. Manson, P. Delaney, F. Jelezko, J. Wrachtrup, and L.C.L. Hollenberg. The nitrogen-vacancy colour centre in diamond. page 101, 2 2013. URL <http://arxiv.org/abs/1302.3288>.
- [5] Richard P. Feynman. Simulating physics with computers. *International Journal of Theoretical Physics*, 21(6-7):467–488, 6 1982. ISSN 0020-7748. URL <http://link.springer.com/10.1007/BF02650179>.
- [6] Adam Gali. Identification of individual  $^{13}\text{C}$  isotopes of nitrogen-vacancy center in diamond by combining the polarization studies of nuclear spins and first-principles calculations. *Physical Review B*, 80(24):241204, 12 2009. ISSN 1098-0121. URL <http://link.aps.org/doi/10.1103/PhysRevB.80.241204>.
- [7] Adam Gali, Maria Fyta, and Efthimios Kaxiras. Ab initio supercell calculations on nitrogen-vacancy center in diamond: Electronic structure and hyperfine tensors. *Physical Review B*, 77(15):155206, 4 2008. ISSN 1098-0121. URL <http://link.aps.org/doi/10.1103/PhysRevB.77.155206>.
- [8] Bas Jorrit Hensen. *Measurement-based Quantum Computation with the Nitrogen-Vacancy centre in Diamond*. PhD thesis, Delft University of Technology, 2011.
- [9] F. Jelezko, T. Gaebel, I. Popa, a. Gruber, and J. Wrachtrup. Observation of coherent oscillations in a single electron spin. *Physical Review Letters*, 92(7):076401, 2 2004. ISSN 0031-9007. URL <http://link.aps.org/doi/10.1103/PhysRevLett.92.076401>.
- [10] W. Pfaff. *Quantum Measurement and Entanglement of Spin Quantum Bits in Diamond*. PhD thesis, Delft University of Technology, 2013.
- [11] L. Robledo, L. Childress, H. Bernien, B. Hensen, P.F.A. Alkemade, and R. Hanson. High-fidelity projective read-out of a solid-state spin quantum register. *Nature*, 477(7366):574–8, 9 2011. ISSN 1476-4687. URL <http://www.ncbi.nlm.nih.gov/pubmed/21937989>.
- [12] P.W. Shor. Algorithms for quantum computation: discrete logarithms and factoring. In *Proceedings 35th Annual Symposium on Foundations of Computer Science*, pages 124–134. IEEE Comput. Soc. Press, 1994. ISBN 0-8186-6580-7. URL <http://ieeexplore.ieee.org/lpdocs/epic03/wrapper.htm?arnumber=365700>.

- [13] Benjamin Smeltzer, Lilian Childress, and Adam Gali.  $^{13}\text{C}$  hyperfine interactions in the nitrogen-vacancy centre in diamond. *New Journal of Physics*, 13(2):025021, 2 2011. ISSN 1367-2630. URL <http://stacks.iop.org/1367-2630/13/i=2/a=025021?key=crossref.bdd6956722cde89a36ab3eee44a82724>.
- [14] T. H. Taminiau, J. J. T. Wagenaar, T. van der Sar, F. Jelezko, V. V. Dobrovitski, and R. Hanson. Detection and control of individual nuclear spins using a weakly coupled electron spin. *Physical Review Letters*, 109(13):137602, 9 2012. ISSN 0031-9007. URL <http://link.aps.org/doi/10.1103/PhysRevLett.109.137602>.
- [15] T. H. Taminiau, J.J.T. J. T. Wagenaar, T. van der Sar, F. Jelezko, V.V. V. Dobrovitski, and R. Hanson. Detection and control of individual nuclear spins using a weakly coupled electron spin. *Physical Review Letters*, 109(13):137602, 9 2012. ISSN 0031-9007. URL <http://link.aps.org/doi/10.1103/PhysRevLett.109.137602><http://arxiv.org/abs/1205.4128>.
- [16] T. H. TH Taminiau, J. Cramer, T. van der Sar, V. V. Dobrovitski, and R. Hanson. Universal control and error correction in multi-qubit spin registers in diamond. *Nature Nanotechnology*, 2(February):2–7, 9 2014. ISSN 1748-3387. URL <http://arxiv.org/abs/1309.5452><http://www.nature.com/doifinder/10.1038/nnano.2014.2>.
- [17] L M Vandersypen, Matthias Steffen, Gregory Breyta, Costantino S Yannoni, Mark H Sherwood, and Isaac L Chuang. Experimental realization of shor’s quantum factoring algorithm using nuclear magnetic resonance. *Nature*, 414(6866):883–7, 2001. ISSN 0028-0836. URL <http://www.ncbi.nlm.nih.gov/pubmed/11780055>.

## Fingerprintdata

The estimated hyperfine parameters of all 13 identified spins can be found in table A.1. Due to the size of the fingerprint analysis it is not possible to include with this thesis. A pdf file containing the fingerprint analysis can be found here: <https://www.dropbox.com/s/giej9e86bfvsf1/fingerprinting.pdf>.

Carbon	$A_{\parallel}$	$A_{\perp}$
1	$2\pi \cdot 30.0$ kHz	$2\pi \cdot 80.0$ kHz
2	$2\pi \cdot 27.0$ kHz	$2\pi \cdot 28.5$ kHz
3	$2\pi \cdot -51.0$ kHz	$2\pi \cdot 105.0$ kHz
4	$2\pi \cdot 45.1$ kHz	$2\pi \cdot 20$ kHz
5	$2\pi \cdot 17$ kHz,	$2\pi \cdot 10$ kHz
6	$2\pi \cdot -15$ kHz,	$2\pi \cdot 12$ kHz
7	$2\pi \cdot -23$ kHz,	$2\pi \cdot 12$ kHz
8	$2\pi \cdot 10$ kHz,	$2\pi \cdot 8.0$ kHz
9	$2\pi \cdot 8.0$ kHz	$2\pi \cdot 12$ kHz
10	$2\pi \cdot -9.3$ kHz	$2\pi \cdot 13$ kHz
11	$2\pi \cdot -10.0$ kHz	$2\pi \cdot 5$ kHz
12	$2\pi \cdot -30.0$ kHz	$2\pi \cdot 35$ kHz
13	$2\pi \cdot -32.0$ kHz	$2\pi \cdot 20$ kHz

**Table A.1** – Estimated hyperfine parameters for spins 1 to 13.





B

**State Initialization**



C

## Bell State Tomography

Derivation, what would a tomography of the  $\Psi^+$  state look like?



D

**Entanglement witness**





## Simulations

Lorem ipsum dolor sit amet, consectetur adipisicing elit, sed do eiusmod tempor incididunt ut labore et dolore magna aliqua. Ut enim ad minim veniam, quis nostrud exercitation ullamco laboris nisi ut aliquip ex ea commodo consequat. Duis aute irure dolor in reprehenderit in voluptate velit esse cillum dolore eu fugiat nulla pariatur. Excepteur sint occaecat cupidatat non proident, sunt in culpa qui officia deserunt mollit anim id est laborum.





## Acknowledgements

Lorem ipsum dolor sit amet, consectetur adipisicing elit, sed do eiusmod tempor incididunt ut labore et dolore magna aliqua. Ut enim ad minim veniam, quis nostrud exercitation ullamco laboris nisi ut aliquip ex ea commodo consequat. Duis aute irure dolor in reprehenderit in voluptate velit esse cillum dolore eu fugiat nulla pariatur. Excepteur sint occaecat cupidatat non proident, sunt in culpa qui officia deserunt mollit anim id est laborum.